Cloud properties derived from two lidars over the ARM SGP site

Jean-Charles Dupont,[1] Martial Haeffelin,[1] Yohann Morille,[2] Jennifer M. Comstock,[3] Connor Flynn,[3] Charles N. Long,[3] Chitra Sivaraman,[3] and Rob K. Newson[3]

Received 24 November 2010; revised 9 February 2011; accepted 15 February 2011; published 29 April 2011.

[1] Active remote sensors such as lidars or radars can be used with other data to quantify the cloud properties at regional scale and at global scale. Relative to radar, lidar remote sensing is sensitive to very thin and high clouds but has a significant limitation due to signal attenuation in the ability to precisely quantify the properties of clouds with a cloud optical thickness larger than 3. The cloud properties for all levels of clouds are derived and distributions of cloud base height (CBH), top height (CTH), physical cloud thickness (CT), and optical thickness (COT) from local statistics are compared. The goal of this study is (1) to establish a climatology of macrophysical and optical properties for all levels of clouds observed over the ARM SGP site and (2) to estimate the discrepancies between the two remote sensing systems (pulse energy, sampling, resolution, etc.). Our first results tend to show that the MPL, which are the primary ARM lidars, have a distinctly limited range within which all of these cloud properties are detectable, especially cloud top and cloud thickness, but this can include cloud base particularly during summer daytime period. According to the comparisons between RL and MPL, almost 50% of situations show a signal to noise ratio too low (smaller than 3) for the MPL in order to detect clouds higher than 7km during daytime period in summer. Consequently, the MPL-derived annual cycle of cirrus cloud base (top) altitude is biased low, especially for daylight periods, compared with those derived from the RL data, which detects cloud base ranging from 7.5 km in winter to 9.5 km in summer (and tops ranging from 8.6 to 10.5 km). The optically thickest cirrus clouds (COT > 0.3) reach 50% of the total population for the Raman lidar and only 20% for the Micropulse lidar due to the difference of pulse energy and the effect of solar irradiance contamination. A complementary study using the cloud fraction derived from the Micropulse lidar for clouds below 5 km and from the Raman lidar for cloud above 5 km allows for better estimation of the total cloud fraction between the ground and the top of the atmosphere. This study presents the diurnal cycle of cloud fraction for each season in comparisons with Long et al.'s (2006) cloud fraction calculation derived from radiative flux analysis. **Citation:** Dupont, J.-C., M. Haeffelin, Y. Morille, J. M. Comstock, C. Flynn, C. N. Long, C. Sivaraman, and R. K. Newson (2011), Cloud properties derived from two lidars over the ARM SGP site, *Geophys. Res. Lett.*, *38*, L08814, doi:10.1029/2010GL046274.

[1]Institut Pierre Simon Laplace, Ecole Polytechnique, Palaiseau, France.
[2]Laboratoire de Météorologie Dynamique, Institut Pierre Simon Laplace, Ecole Polytechnique, Palaiseau, France.
[3]Pacific Northwest National Laboratory, Richland, Washington, USA.

0094-8276/11/2010GL046274

1. Introduction

[2] A unique Raman lidar is installed at the ARM SGP site [*Stokes and Schwartz*, 1994; *Ackerman and Stokes*, 2003] site that permits us to observe the atmospheric column between 1 and 20 km [*Turner et al.*, 2002]. Multiple Micropulse lidars are installed at ARM SGP, Tropical Western Pacific (TWP) and North Slope of Alaska (NSA) sites and are characterized by a limited sensitivity during daytime period, especially for high altitude clouds.

[3] The objective of this study is to characterize the all-level cloud properties over the ARM SGP site and to quantify the consistency between the Micropulse (MPL) and the Raman (RL) lidar with altitude. In this study, 10-years of backscatter lidar signal data are analysed by a unique algorithm called STRucture of ATmosphere (STRAT) [*Morille et al.*, 2007]. STRAT is designed to retrieve the vertical distribution of cloud and aerosol layers in the boundary layer and through the free troposphere and to identify near-particle-free regions of the vertical profile and the range at which the lidar signal becomes too attenuated for exploitation, from a single lidar channel. We apply the STRAT algorithm to data from both the collocated Micropulse lidar (MPL) and a Raman lidar (RL) between 1998 and 2009. Raw backscatter lidar signal is processed and corrections for detector deadtime, afterpulse, and overlap are applied [*Campbell et al.*, 2002].

2. Observations Data Set, Sampling and Case Study

[4] Micropulse lidar and Raman lidar characteristics are presented in the Table 1. For the micropulse lidar, *Campbell et al.* [2002] corrections have been manually applied for dead-time, overlap and after-pulse errors on the raw data available on ARM web site. Prior to a major refurbishment of the Raman lidar in 2004, the electronics were limited to only photon counting data acquisition. These data were acquired with a range resolution of 39 m and a temporal resolution of 1 min [*Goldsmith et al.*, 1998]. In 2004 the system underwent a major refurbishment [*Ferrare et al.*, 2006], which included replacement of the existing data system with new data recorders capable of simultaneous photon counting and analog detection [*Newsom et al.*, 2009]. The new data system improved the spatial and temporal resolution to 7.5 m and 10 s, respectively. For this study, raw signal processing consists having deadtime correction before June 2004 and adding the merging of photon counting and analog signals [*Newsom et al.*, 2009]. We also point out that no overlap correction has been applied to the raw Raman lidar data for this study. For the wide Field Of View (narrow FOV) channels, complete overlap is achieved at a height of about 800 m (4 km).

Table 1. Micropulse and Raman Lidar Characteristics

	Micropulse Lidar	Raman Lidar
Laser type	Nd-YLF	Nd-Yag
Emitted wavelengths	523 nm	355 nm
Pulse energy	10 μJ	300–320 mJ
Repetition rate	2500 Hz	30 Hz
Resolution	30m/1min	39 m/5 min − 37.5m/2min
Telescope	Ø = 20cm	Ø = 61cm
	FOV = 0.1 mrad	FOV = 0.3 mrad

[5] The annual sampling of MPL and RL between 1998 and 2009 are presented in the Table 2. We use here the number of hours of observations to normalize according to the raw lidar sampling. We note a more homogeneous sampling for MPL before 2003 compared to RL. The year 2007 and 2008 are better for the RL due to the new system of measurement.

3. Results and Discussion

3.1. Usable Lidar Signal

[6] Figure 1 shows the diurnal cycle of the usable signal for the MPL (Figure 1, right) and the RL (Figure 1, left) distinguishing winter and summer seasons. The MPL is very sensitive to the solar background noise with only 50% of usable signal at a height of 7 km during summer. The solar contribution is hence a major problem during summer for MPL whereas we note only a very limited impact for the Raman lidar. The usable lidar signal corresponds to a signal with a signal to noise ratio bigger than 3 [*Morille et al.*, 2007] for the parallel signal. We do not use here the depolarization ratio. To compare unbiased statistics between MPL and RL, we account for this usable lidar signal in order to be sure that all clouds would be detected. For the daytime period during summer, the maximum cloud base height for comparisons would be 4–5 km.

3.2. Cloud Altitude

[7] Figure 2 shows the annual cycle of the cloud base height (CBH) and cloud top height (CTH) over the SGP site derived from the MPL (red line) and the RL (black line) for the clouds higher than 5 km. This statistic includes only the time period when we are confident with the lidar signal (i.e., the lidar "sees" through the entire cloud) and when we have coincident measurement between MPL and RL. The dashed line corresponds to the nighttime period and solid line to the daytime period. The average CBH, in merging day and night, is equal to 8.2 km for RL and MPL whereas the CBH and CTH annual cycle are much more significant for RL than for the MPL. The diurnal cycle for the CBH and CTH is quasi null for the MPL due to the very limited range of the sensitivity especially during the summer period. Consequently, the agreement is good for the winter period (CBH~7.7 km, CTH~9.1 km) and the difference is bigger than 1km for the summer period.

3.3. Multiple Cloud Layers

[8] The STRAT algorithm is able to detect up to 6 cloud layers if the lidar signal is not too attenuated. The results are very similar for the MPL and the RL with a maximum difference of 4% concerning the comparisons for the detection of only one cloud layer occurrence (except for 2003 because of the very limited sampling for the RL, i.e., difference of 10%). Over SGP site, one cloud layer is detected on average 73% of the time for both the MPL and RL. However, we note a shift of 10% between the 1998–2003 period and the 2003–2009 period. One cloud layer represents 78% of the situations before 2003 and 68% after 2003. A second cloud layer appears in 18% of the cloudy profiles before 2003 and 25% after 2003 and a third (or more) cloud layer 4% before and 7% after 2003. The less sensitive MPL signal does not cause significant difference for the detection of the number of different cloud layers. The comparisons for daytime and nighttime period for the MPL show an occurrence of multiple cloud layer 10% stronger during the night related to absence of the sun radiation inducing significant impact on the MPL signal to noise ratio. We note no difference for the RL day and night comparisons.

3.4. Cloud Fraction

[9] The two means used here to derive the cloud are the hemispheric and the column techniques. In the former case, the downwelling shortwave or longwave radiation at the surface is interpreted to derive cloudiness. This measure is generally referred to as fractional sky cover, and is understood to be an angular measure of what portion of the hemispheric view contains cloud elements. We distinguish here the cloud fraction derived from the shortwave fluxes (CFSW) [*Long et al.*, 2006] and from the longwave fluxes (CFLW) [*Long and Turner*, 2008; *Durr and Philipona*, 2004]. In the latter case the instrument by nature is insensitive to high, cold clouds and thus senses primarily only the low and middle cloudiness. For vertically pointing instruments such as lidars, a time series analysis is used to calculate the fraction of the total time that cloud elements are detected by the observing instrument. This "cloud time fraction" is then assumed to represent the nadir projected area cloud fraction, i.e., the portion of the surface that is shaded if the clouds are illuminated from directly above *Kassianov et al.* [2005]. The total cloud fraction derived from the lidars (CFTOT) accounts for the multiple cloud layers (occurring between 22 and 32% of the time, paragraph [8]) in order to calculate a unique cloud fraction for the whole atmospheric column.

[10] The *volumic* cloud fraction is defined as the number of cloudy pixels detected by STRAT inside the box of 150 m x 1 hour. Here, we use only the RL dataset in order to have complete information between the surface and 15 km high. Figure 3 shows the *volumic* cloud fraction derived from RL data over the SGP site. It corresponds to the average value of cloud fraction for two different seasons (winter and

Table 2. Annual Lidar Retrievals for the Micropulse and Raman Lidars[a]

Year	1998	1999	2000	2001	2002	2003	2004	2005	2006	2007	2008	2009
RL	2700	2400	3300	5200	3500	1200	2150	6700	8200	5600	7800	3500
MPL	/	5100	4900	5050	7150	5250	7600	7500	5000	/	/	/

[a]Unit: hours.

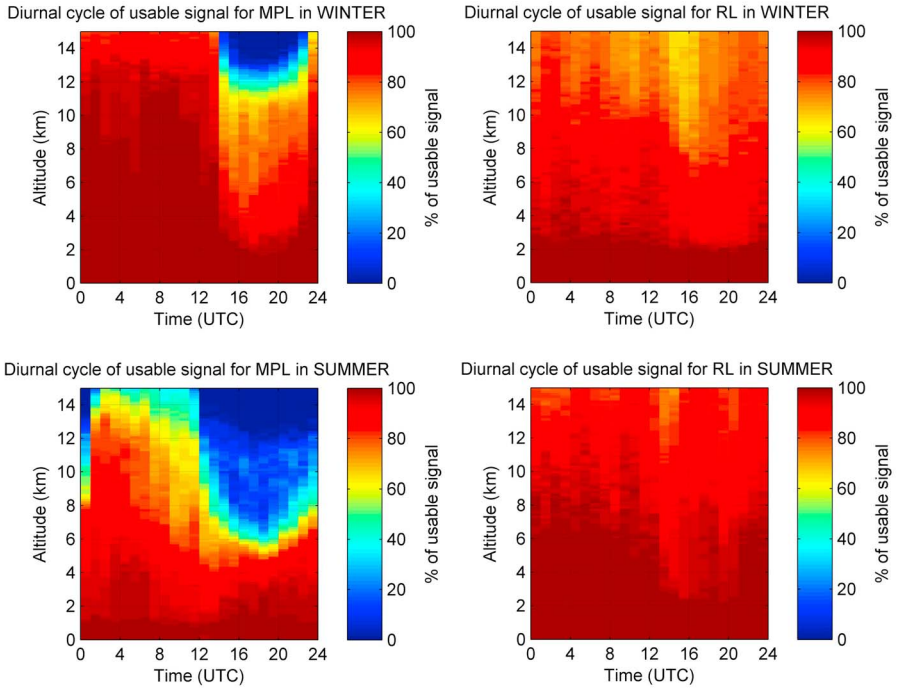

Figure 1. Diurnal cycle of the usable signal for the (right) Micropulse and the (left) Raman lidar distinguishing winter and summer seasons.

summer) between 1998 and 2009. The major seasonal differences concern the low altitude clouds (i.e., 2 km < CBH < 5 km). The relative occurrence for these clouds is 15% for winter, 22% for spring, 11% for summer and 13% for fall. The cumulus clouds appear for the summer period at 3 km high between 0900 UT and 1200 UT. The biggest relative occurrence appears for the period between 0000 UT and 0600 UT concerning the very high altitude clouds with a CBH near 8 to 10 km.

[11] The *surfacic* cloud fraction is defined as the number of 5 min or 2 min lidar profiles classified as cloudy divided by total number of profiles during a 1 hour period. For the results provided in Figure 1, we use the MPL to derive the low-level cloud fraction (CF_{MPL}) concerning cloud base height below 5 km high and the RL to derive the complementary cloud fraction higher than 5 km (CF_{RL}). Both lidar systems have difficulty detecting clouds below 0.5 km high so we are unable to give information for fog or low stratus cloud for example.

[12] Figure 3 on the right shows the *surfacic* cloud fraction. Average values for the winter period (summer period) is CFMPL = 25% (31%), CFRL = 29% (31%), CFSW = 48% (42%), CFLW = 35% (37%) and CFTOT = 52% (52%). The daytime cloud fraction derived from shortwave analysis is smaller than the total cloud fraction provided by the lidar method especially during the summer period (8%). This phenomenon can be explained by the fact that the shortwave radiative method is not very sensitive to very thin cirrus cloud of optical depths of about 0.15 or less [*Dupont et al.*, 2010], more numerous during the summer period. Cloud optical thickness of residual clouds not detected by the shortwave radiative method is here calculated (not

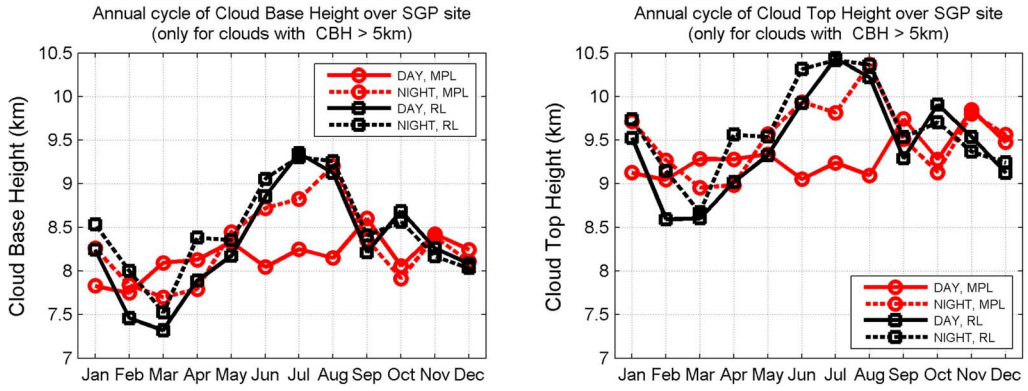

Figure 2. Annual cycle of the cloud base height and cloud top height over the SGP site derived from the Micropulse lidar (red line) and the Raman lidar (black line). Dashed line corresponds to the nighttime period and continuous line to the daytime period.

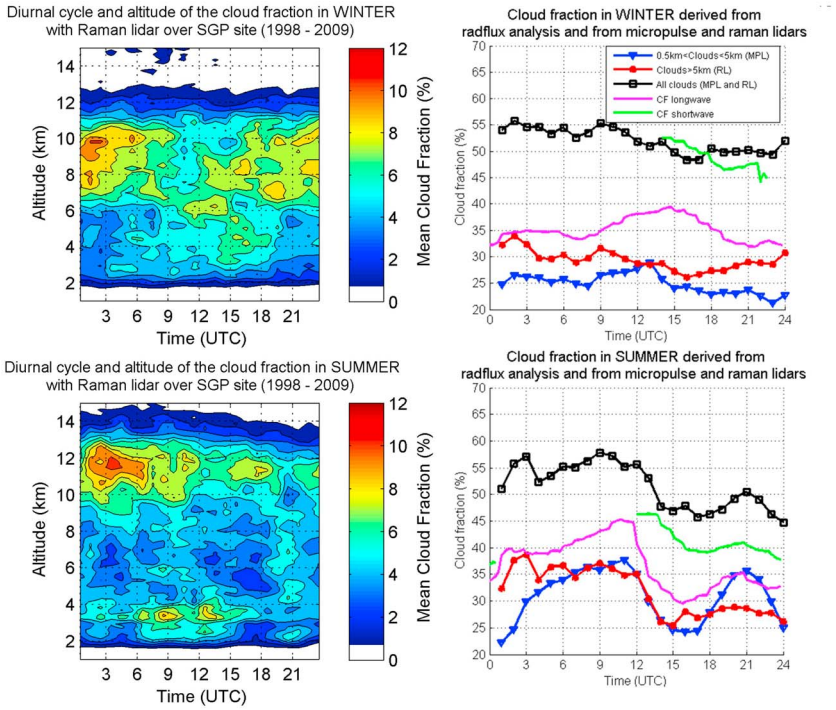

Figure 3. Volumic and surfacic cloud fraction derived from Raman lidar data over SGP site. It corresponds to the average value of cloud fraction for 2 different seasons between 1998 and 2009.

shown) by the [*Cadet et al.*, 2005] method. It confirms that around 15–20% of these clouds have optical thicknesses smaller than 0.15–0.20. The CFLW is quite similar to the CFMPL during the summer period (6% difference) whereas we note a stronger residual error for the winter period (10% difference). This difference of 4% between summer and winter is likely due the stratus clouds and fog lower than 0.5 km (more frequent in winter) not accounted for in the MPL method. The residual difference around 6% (relatively constant) between lidar and longwave irradiance algorithm cloud fractions during daytime and nighttime period is most likely due to the cirrus cloud signal too small for the longwave measurements.

[13] The summer period is characterized by a significant diurnal cycle of the low level clouds with a maximum cloud fraction reaching almost 38% at 10:00 and 20:00 and a minimum of 20% at 00:00 and 15:00. This diurnal variation, also seen in the radiative flux analysis, is explained by the frequency of cumulus cloud development in the summer.

3.5. Cloud Optical Thickness

[14] The cloud optical thickness is here derived using the Molecular Integration (MI) method starting from the lidar backscatter signal [*Cadet et al.*, 2005]. Cloud optical thickness derived from lidar measurement is affected by the significant extinction of the lidar beam in its path through the medium, and in most situations, one must take into account multiple scattering. Some typical values of multiple scattering factor η, as given by *Chen et al.* [2002] are η = 0.58 for COT = 1 and η = 0.95 for COT = 0.1. *Sassen and Comstock* [2001] assume that the multiple scattering factor is of 0.9 for subvisible cirrus clouds, of 0.8 for relatively thick clouds, and of 0.6 to 0.7 for optically thick clouds. For this study, we consider *Chen et al.*'s [2002] parametric equation which accounted for a major part of the multiple scattering effect on the COT retrievals.

[15] A major upgrade of the Raman lidar occurred in 2004 which induced a significant improvement especially for the signal to noise ratio and so could have a strong impact on the cloud optical thickness retrievals. We decide to analysis separately the "old" and the "new" COT retrieval for the Raman lidar. The "old" (and the "new") RL COT are larger than the MPL retrievals: 55% (40%) of clouds are thick (i.e., COT > 0.3) for RL and only 20% for MPL; 41% (53%) are semi-transparent clouds (i.e., 0.03 < COT < 0.3) for RL and almost 66% for MPL and finally 4% (7%) are subvisible clouds (i.e., COT < 0.03) for RL and 14% for MPL. These statistics are biased by the much better sensitivity of the Raman lidar to the lowest and optically thickest clouds (the RL pulse energy is 30000 times bigger than the MPL). However, the 2004 upgrade does not modulate significantly the ratio thick/subvisible/thin clouds although the signal to noise ratio is much better. For the clouds below 5 km high, the relative occurrence of the optically thick cloud reaches 80% 68%) for RL and only 40% for MPL, hence a difference of 40% (28%) against 35% (20%) for all clouds.

4. Conclusions

[16] This first study allows us to precisely quantify the agreement between two lidars in using only one algorithm named STRAT [*Morille et al.*, 2007]. The major conclusions are:

[17] 1. The MPL has a limited range compared to the RL and this creates difficulties in the detection of high clouds, especially during daytime and summer periods: 2 km bias appeared for high cloud.

[18] 2. During the winter period, the shortwave cloud fraction compares well with the lidar method because it is likely dominated by low-level stratus, which is generally totally overcast, particularly in the morning hours. During the summer, the radiative flux analysis shows less cloud fraction because it is not sensitive to thin cirrus (optical thickness smaller than 0.15), which is more prevalent in the spring/summer months.

[19] 3. 50% of all clouds have a moderate cloud optical thickness (COT > 0.3) for Raman lidar against only 20% for micropulse lidar due to the lack of sensitivity for high altitude clouds.

[20] Basically, users of ARM MPL data should be aware that during daylight hours the increased noise from solar scattering at the lidar wavelength in essence poses a significant limit on the height of clouds that can be detected. Thus one must exercise caution in using MPL-generated cloud statistics as "truth" especially for high cloud occurrence, as it will be underestimated.

[21] Future work consists in quantifying the cloud properties over ARM TWP and ARM NSA sites derived from MPL lidar and STRAT algorithm.

[22] **Acknowledgments.** The authors would like to thank the Centre National de la Recherche Scientifique (CNRS) and the Pacific Northwest National Laboratory (PNNL) for their support in this study. The authors from PNNL acknowledge the support of the Climate Change Research Division of the U.S. Department of Energy as part of the Atmospheric Radiation Measurement (ARM) and Atmospheric System Research (ASR) Programs. We extend our acknowledgments to the technical and computer staff of each observatory for taking the observations and making the data set easily accessible. The authors are grateful to the anonymous reviewers for their useful comments.

[23] The Editor would like to thank the two anonymous reviewers for their assistance in evaluating this paper.

References

Ackerman, T. P., and G. M. Stokes (2003), The Atmospheric Radiation Measurement Program, *Phys. Today*, *56*, 38–44, doi:10.1063/1.1554135.

Cadet, B., V. Giraud, M. Haeffelin, P. Keckhut, A. Rechou, and S. Baldy (2005), Improved retrievals of cirrus cloud optical properties using a combination of lidar methods, *Appl. Opt.*, *44*, 1726–1734, doi:10.1364/AO.44.001726.

Campbell, J. R., D. L. Hlavka, E. J. Welton, C. J. Flynn, D. D. Turner, J. D. Spinhirne, V. S. Scott, and I. H. Hwang (2002), Full-time, eye-safe cloud and aerosol lidar observation at Atmospheric Radiation Measurement Program sites: Instruments and data processing, *J. Atmos. Oceanic Technol.*, *19*, 431–442, doi:10.1175/1520-0426(2002)019<0431:FTESCA>2.0.CO;2.

Chen, W. N., C. W. Chiang, and J. B. Nee (2002), Lidar ratio and depolarisation ratio for cirrus clouds, *Appl. Opt.*, *41*, 6470–6476, doi:10.1364/AO.41.006470.

Dupont, J. -C., M. Haeffelin, Y. Morille, V. Noël, P. Keckhut, D. Winker, J. Comstock, P. Chervet, and A. Roblin (2010), Macrophysical and optical properties of midlatitude cirrus clouds from four ground-based lidars and collocated CALIOP observations, *J. Geophys. Res.*, *115*, D00H24, doi:10.1029/2009JD011943.

Durr, B., and R. Philipona (2004), Automatic cloud amount detection by surface longwave downward radiation measurements, *J. Geophys. Res.*, *109*, D05201, doi:10.1029/2003JD004182.

Ferrare, R. A., et al. (2006), Evaluation of daytime measurements of aerosols and water vapor made by an operational Raman lidar over the Southern Great Plains, *J. Geophys. Res.*, *111*, D05S08, doi:10.1029/2005JD005836.

Goldsmith, J. E. M., F. H. Blair, S. E. Bisson, and D. D. Turner (1998), Turn-key Raman lidar for profiling atmospheric water vapor, clouds and aerosols, *Appl. Opt.*, *37*, 4979–4990, doi:10.1364/AO.37.004979.

Long, C. N., and D. D. Turner (2008), A method for continuous estimation of clear-sky downwelling longwave radiative flux developed using ARM surface measurements, *J. Geophys. Res.*, *113*, D18206, doi:10.1029/2008JD009936.

Long, C. N., T. P. Ackerman, K. L. Gaustad, and J. N. S. Cole (2006), Estimation of fractional sky cover from broadband shortwave radiometer measurements, *J. Geophys. Res.*, *111*, D11204, doi:10.1029/2005JD006475.

Morille, Y., M. Haeffelin, P. Drobinski, and J. Pelon (2007), STRAT: An automated algorithm to retrieve the vertical structure of the atmosphere from single-channel lidar data, *J. Atmos. Oceanic Technol.*, *24*, 761–775, doi:10.1175/JTECH2008.1.

Newsom, R. K., D. D. Turner, B. Mielke, M. F. Clayton, R. Ferrare, and C. Sivaraman (2009), Simultaneous analog and photon counting detection for Raman lidar, *Appl. Opt.*, *48*, 3903–3914, doi:10.1364/AO.48.003903.

Sassen, K., and J. Comstock (2001), A midlatitude cirrus cloud climatology from the facility for atmospheric remote sensing. Part III: Radiative properties, *J. Atmos. Sci.*, *58*, 2113–2127, doi:10.1175/1520-0469(2001)058<2113:AMCCCF>2.0.CO;2.

Stokes, R. R., and S. E. Schwartz (1994), The Atmospheric Radiation Measurement (ARM) Program: Programmatic background and design of the Cloud and Radiation Test Bed, *Bull. Am. Meteorol. Soc.*, *75*, 1201–1222, doi:10.1175/1520-0477(1994)075<1201:TARMPP>2.0.CO;2.

Turner, D. D., R. A. Ferrare, L. A. Heilman Brasseur, W. F. Feltz, and T. P. Tooman (2002), Automated retrievals of water vapor and aerosol profiles from an operational Raman lidar, *J. Atmos. Oceanic Technol.*, *19*, 37–50, doi:10.1175/1520-0426(2002)019<0037:AROWVA>2.0.CO;2.

J. M. Comstock, C. Flynn, C. N. Long, R. K. Newson, and C. Sivaraman, Pacific Northwest National Laboratory, 3200 Q Ave., Richland, WA 99352, USA.

J.-C. Dupont and M. Haeffelin, Institut Pierre Simon Laplace, Ecole Polytechnique, F-91128 Palaiseau CEDEX, France. (jean-charles.dupont@ipsl.polytechnique.fr)

Y. Morille, Laboratoire de Météorologie Dynamique, Institut Pierre Simon Laplace, Ecole Polytechnique, F-91128, Palaiseau CEDEX, France.